Triblock Copolymer Organogels as High-Performance Dielectric Elastomers

Ravi Shankar,[†,‡,⊥] Arjun K. Krishnan,[§] Tushar K. Ghosh,[†] and Richard J. Spontak*[,‡,§]

Fiber and Polymer Science Program and Departments of Materials Science & Engineering and Chemical & Biomolecular Engineering, North Carolina State University, Raleigh, North Carolina 27695

Received August 22, 2007; Revised Manuscript Received November 16, 2007

ABSTRACT: Block copolymers and nanostructured materials derived therefrom are becoming increasingly ubiquitous in a wide variety of (nano)technologies. Recently, we have demonstrated that triblock copolymer organogels composed of physically cross-linked copolymer networks swollen with a midblock-selective solvent exhibit excellent electromechanical behavior as dielectric elastomers. In-plane actuation of such organogels, collectively referred to as electroactive nanostructured polymers (ENPs) to reflect the existence of a self-organized copolymer morphology, is attributed to the development of an electric-field-induced surface-normal Maxwell stress. In this study, we examine the composition and molecular weight dependence of the electromechanical properties afforded by organogels prepared from poly[styrene-*b*-(ethylene-*co*-butylene)-*b*-styrene] (SEBS) triblock copolymers selectively swollen with EB-compatible aliphatic oligomers. These materials undergo ultrahigh actuation displacement at significantly reduced electric fields relative to previously reported dielectric elastomers and possess electromechanical coupling efficiencies, which relate the conversion from electrical input to mechanical output, greater than 90%. The design of ENPs with broadly tunable electromechanical properties represents an attractive route to responsive materials for advanced engineering, biomimetic and biomedical applications.

Introduction

Triblock copolymers consisting of chemically distinct homopolymers that are covalently linked in an ABA sequence are capable of spontaneous self-organization into a variety of classical nanoscale morphologies such as lamellae, cylinders on a hexagonal lattice, and spheres on a body-centered-cubic lattice,[1−3] as well as spatially complex morphologies such as the gyroid[4] and sponge,[5] alone or in the presence of a solvent, homopolymer, or another copolymer. Generally speaking, nanostructured block copolymers provide a remarkably broad platform for the development of multifunctional materials targeted for various (nano)technologies[6,7] including, for instance, nanotemplates,[8] membranes,[9] nanoporous media,[10] and biomaterials.[11] Most notably, ABA triblock copolymers have been used extensively as thermoplastic elastomers[2,12] (TPEs) due to their shape-memory attributes. Addition of an organic solvent to a microphase-separated AB diblock[13] or ABA triblock[14] copolymer provides a straightforward route by which to controllably modify copolymer morphologies and accompanying properties. Unlike their AB diblock counterparts, however, ABA molecules are capable of connecting neighboring microdomains via midblock bridges and thus generating physically cross-linked molecular networks (schematically depicted in Figure 1a) in the presence of a B-selective solvent.[15−22] At relatively high concentrations of a B-selective solvent, the incompatible A blocks of the ABA molecules aggregate to form spherical micelles (cf. Figure 1b), which serve to stabilize the copolymer network and thereby generate an organogel.

Organogels derived from commercial TPEs are ideally suited for diverse applications ranging from personal care and other consumer products to vibration-dampening media and adhesives.

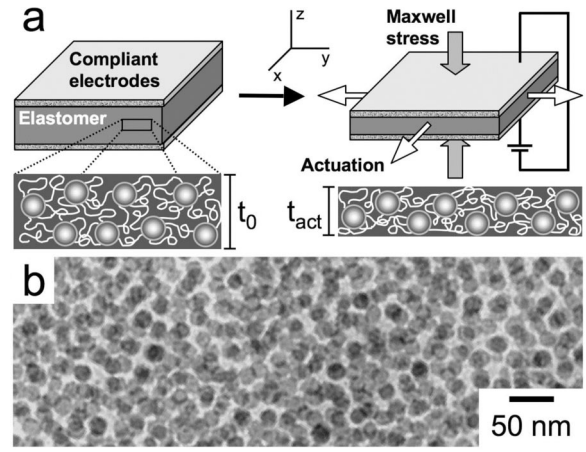

Figure 1. In (a), a schematic diagram of the mechanism by which a dielectric elastomer actuates upon electrical stimulation. The electric-field-induced Maxwell stress and resulting in-plane actuation (along *x* and *y*) are labeled. Included are pre- and post-actuation illustrations of the micellar morphology present in selectively swollen triblock copolymer organogels introduced as electroactive nanostructured polymers (ENPs). In (b), a TEM image of the micellar morphology generated in a 10/90 w/w SEBS/MO blend. The styrenic units comprising the micellar core are stained with the vapor of RuO_4(aq) and appear dark.

Recently, we have reported[23−25] that such organogels likewise exhibit excellent electromechanical behavior as dielectric elastomers. Dielectric elastomers comprise one class of electroactive polymers (EAPs), macromolecules that respond to external electrical stimulation by displaying a significant change in shape or size and thus converting electrical energy into mechanical force and movement.[26] Because of their lightweight, mechanical resilience, low cost, and facile processability, EAPs constitute excellent candidates for use in micro-air vehicles, microrobotics, microfluidic/haptic devices, active displays, and responsive prosthetics.[27] Actuators derived from EAPs possess higher energy density, response speed, and electromechanical coupling

* To whom correspondence should be sent: e-mail Rich_Spontak@ncsu.edu.
[†] Fiber and Polymer Science Program.
[‡] Department of Materials Science & Engineering.
[§] Department of Chemical & Biomolecular Engineering.
[⊥] Current address: Assembly & Test Technology Development Division, Intel Corporation, Chandler, AZ 85226.

10.1021/ma071903g CCC: $40.75
Published on Web 07/12/2008

efficiency than inorganic actuators such as piezoelectric ceramics.[28] Common EAPs include conductive[28] and ferroelectric[29,30] polymers, in addition to carbon nanotubes[31] and dielectric elastomers. Of all the EAPs investigated thus far, though, dielectric elastomers exhibit the largest actuation displacement (>100% on an area basis[32]) but typically require high electric fields (ca. 50−250 V/μm) to achieve full actuation. These elastomers are traditionally produced from chemically cross-linked homopolymers, and the two most promising EAPs in this genre derive specifically from acrylic and silicone elastomers, with the former serving as the benchmark due to its exceptional electromechanical properties.[26,33]

Although experimental and theoretical studies have endeavored to elucidate the response of microphase-separated block copolymers to an applied electric field, such efforts have focused exclusively on (re)alignment of the copolymer nanostructure in both thin[34] and bulk[35] films with and without solvent. In our previous study,[23] we have demonstrated that organogels composed of nonpolar poly[styrene-*b*-(ethylene-*co*-butylene)-*b*-styrene] (SEBS) triblock copolymers (each with glassy S end blocks and a rubbery EB midblock) swollen with an EB-selective (aliphatic) solvent exhibit ultrahigh actuation displacement as dielectric elastomers, exceeding the performance benchmarks established by the acrylic elastomer. To distinguish the difference between chemically cross-linked homopolymer-based dielectric elastomers and physically cross-linked copolymer-based elastomers, we refer to the latter as electroactive nanostructured polymers (ENPs) in light of the existing copolymer morphology. The functional effectiveness of ENPs is primarily attributed to their intrinsically low modulus. Moreover, organic functionalities possessing delocalized π-electrons (e.g., the phenyl rings located on the S repeat units of the SEBS copolymer) are known[36] to exhibit nonlinear optical properties and, unlike the EB units and solvent, are polarizable in the presence of a high electric field. The objective of the present study is to interrogate, in systematic fashion, ENPs varying in copolymer molecular weight and concentration to assess the extent to which their electromechanical properties are physically tunable.

Theoretical Background

The actuation response of a dielectric elastomer film is attributed to the development of a Maxwell stress (σ_M) acting normal to the film surface upon electrical stimulation. This predominantly uniaxial compressive stress, or pressure, arises in response to the electrostatic force of attraction between compliant electrodes applied to the opposing surfaces of the film and promotes in-plane (lateral) expansion of the film. According to the continuum model proposed by Pelrine et al.,[26] the effective electrostatic pressure (P) acting along the transverse (z) direction defined in Figure 1 is given by

$$P = \frac{1}{A_{xy}}\frac{dU}{dz} \tag{1}$$

where U denotes the electrostatic potential and A_{xy} is the lateral surface area undergoing compression. For perfectly elastic materials, dU/dz is equal to the mechanical work that can be performed by an actuator. When a potential is applied across the elastomer film, the dielectric elastomer construct depicted in Figure 1a is analogous to a parallel-plate capacitor for which

$$U = \frac{Q^2}{2C} \tag{2}$$

where Q represents the charge on the plate and the capacitance (C) is given by $\epsilon_0\epsilon A_{xy}/z$. Here, ϵ_0 is the permittivity of free space, and ϵ corresponds to the dielectric constant of the elastomer. The change in potential (dU) accompanying concurrent changes in film thickness (dz) and area (dA_{xy}) due to actuation can be determined directly from eq 2, in which case

$$dU = \frac{Q^2}{2\epsilon\epsilon_0}\left(\frac{dz}{A_{xy}} - \frac{z\,dA_{xy}}{{A_{xy}}^2}\right) \tag{3}$$

If the deformation due to actuation is isochoric, $dV = z\,dA_{xy} + A_{xy}\,dz = 0$, and eq 3 simplifies to

$$dU = \frac{Q^2}{\epsilon\epsilon_0}\frac{dz}{A_{xy}} \tag{4}$$

Substitution of eq 4 into eq 1 yields

$$P = \frac{Q^2}{\epsilon\epsilon_0{A_{xy}}^2} \tag{5}$$

Since the electric field (E) is given by $Q/\epsilon_0\epsilon A_{xy}$, the electrostatic pressure, or equivalently σ_M, can be conveniently written as

$$P = \epsilon_0\epsilon E^2 \tag{6}$$

Equation 6 establishes that the field-induced electrostatic stress introduced during actuation is proportional to E^2 and ϵ of the elastomer, the latter of which distinguishes these actuators from other electrostatic materials because the magnitude of ϵ for a polymer can be readily altered (by chemical or physical means) to increase σ_M without increasing the operating voltage. Alternatively, σ_M can be similarly increased by decreasing the thickness of the film (through, for instance, mechanical prestrain) and thus increasing E, which can be equivalently expressed as U/t_0, where t_0 represents the film thickness prior to actuation (cf. Figure 1a). Since σ_M acts normal to the film surface, it serves to compress the film along its thickness (z) and stretch the film laterally (along x and y in Figure 1). Repulsive-like charges accumulate along both film surfaces and further increase the extent to which the film stretches laterally. The resulting transverse strain (s_z) is defined as $(t_{act} - t_0)/t_0$, where t_{act} denotes the dielectric elastomer film thickness after actuation. At sufficiently small strains (<20%), the deformation due to actuation can be presumed to be linearly elastic, and Hooke's law in compression ($\sigma_M = -Ys_z$) can be used to directly relate s_z to the applied electric field, viz.,

$$s_z = -\epsilon\epsilon_0\frac{E^2}{Y} \tag{7}$$

At large strains routinely encountered with dielectric elastomers, however, Y becomes a function of strain so that eq 7 is no longer valid. In the limit of large in-plane (lateral) strains s_x and s_y, s_z can be discerned directly from constitutive relations. Under isochoric conditions, the in-plane and transverse strains are related by $(1 + s_x)(1 + s_y)(1 + s_z) = 1$. If the actuation-induced deformation is laterally isotropic, then $s_x = s_y = s_{xy}$ and

$$s_z = (1 + s_{xy})^{-2} - 1 \tag{8}$$

Actuation of dielectric elastomers is frequently measured using a circular test geometry,[37] which yields the in-plane actuation strain (s_{act}) expressed in terms of the electric field-induced change in electrode area, $(A_{act} - A_0)/A_0$. Again assuming isotropic in-plane actuation, this commonly reported strain is related to s_{xy} by $s_{act} = (1 + s_{xy})^2 - 1$, which consequently requires that

$$s_z = (1 + s_{act})^{-1} - 1 \tag{9}$$

Although s_z has been measured[38] by Doppler interferometry, it is typically computed from s_{act} by eq 9.

Experimental Section

Materials. Three SEBS triblock copolymers with comparable compositions (30−33 wt % S) and different molecular weights (75,

161, and 217 kDa) were used to produce the ENPs investigated in this study. These copolymers were obtained from the GLS Corp. (McHenry, IL), and the corresponding ENPs are hereafter designated as ENP*M*, where *M* (75, 161, and 217) denotes the copolymer molecular weight in kDa. The EB-selective oligomeric solvent, an aliphatic/alicyclic white mineral oil (MO) manufactured as Witco Hydrobrite 380 with a molecular weight of 503 Da by Sonneborn, Inc. (Tarrytown, NY), was used as-received. According to the manufacturer and previous studies,[39] the composition of the MO is estimated to be about 70% paraffinic and 30% naphthenic. The acrylic elastomer, commercialized as a double-sided adhesive (VHB-4910), was obtained in its chemically cross-linked elastomer form from 3 M Co. (St. Paul, MN) and also used as-received.

Methods. Each organogel was prepared by mixing the copolymer with an EB-selective solvent at a predetermined block copolymer concentration (w_{BC}, in wt %), along with 1 wt % antioxidant, for 30 min in a Ross LDM double-planetary mixer under vacuum at 180 °C. The ENP75 systems were produced over the w_{BC} interval from 25 to 50 wt % in 5 wt % increments, whereas w_{BC} in the ENP161 and ENP217 systems ranged from 5 to 30 wt % also in 5 wt % increments. The difference in concentration ranges was due to the melt viscosity of the organogel and the operational limitation of the mixer. A portion of each organogel was compression-molded at 180 °C and then slowly cooled to ambient temperature, yielding films measuring 0.5−2.5 mm thick.

Mechanical Property Characterization. Since the actuation response of elastomers is strongly influenced by their mechanical properties, each of the ENPs prepared during the course of this study, as well as the acrylic dielectric elastomer, was subjected to uniaxial compression and tension testing performed at ambient temperature with an MTS-30G unit operated at cross-head speeds of 5 and 127 mm/min, respectively. Free compression tests were conducted under indirect-contact conditions wherein silicone oil (which is immiscible with the copolymers and aliphatic solvents employed in ENP preparation) was applied to the top and bottom platen prior to measurement. This procedure, which alleviates the development of shear forces during compression, was previously found[40] to yield compressive moduli (Y_C) that were much closer in magnitude to the corresponding tensile moduli (Y_T) than Y_C values measured by direct specimen contact. Another consideration examined here was mechanical hysteresis, which constitutes an important issue in the general design of EAPs intended for cyclic applications (e.g., flapping). The ENPs and acrylic elastomer were cycled up to 400% tensile strain for 100 cycles at a fixed extension rate of 500 mm/min. After 100 cycles, the nonrecoverable strain due to permanent material deformation was assessed.

Electromechanical Property Characterization. The dielectric constants of the ENPs and acrylic elastomer were measured on an Agilent dielectric test fixture 16451B with an HP4284A LCR meter operated over a frequency range of 20 Hz−1 MHz at 25 °C. The actuation response of the dielectric elastomers to an external electric field was investigated under no prestrain and 300% biaxial prestrain conditions in the conventional circular test configuration. Prestrain was necessary to decrease film thickness and thus increase the magnitude of the electric field at manageable electric potentials. Compliant electrodes (Ag silicone grease from Chemtronics Circuit Works, Kennesaw, GA) were applied in a circular pattern (the active area) to the top and bottom surfaces of each film. To avoid boundary effects, this active region (79 mm^2) was kept small (∼1%) relative to the inactive region of the film (7775 mm^2). The quality of selected electrode/ENP/electrode constructs (illustrated in Figure 1a) was evaluated by fracturing the constructs in liquid nitrogen. Cross-sectional backscattered electron (BSE) images were acquired by variable-pressure scanning electron microscopy performed with a Hitachi S-3200N microscope operated under a He atmosphere (100 Pa) at an accelerating voltage of 20 kV. Upon application of a voltage across the electrodes, the active circular region expanded due to transverse film compression. Electric-field-induced actuation was evaluated using a manual voltage trigger, followed by frame-by-frame analysis of captured real-time video images. Image analysis software (Matrox Inspector 4.1) was used to measure the in-plane (lateral) actuation strain (s_{act}) and discern the transverse actuation strain (s_z) under the assumption of isochoric displacement. To discern the extent of hysteresis due to actuation cycling, the voltage across a specimen was ramped from zero to an applied voltage in 10 s, and no noticeable lag was observed between voltage ramping and full specimen actuation. Afterward, the specimen was held at voltage for 10 s before the voltage was returned to zero for 10 s to permit discharge. This process was repeated for 100 cycles, and image analysis was used to compare the size of the active area in the initial image frame with that after 100 cycles and thus discern the extent of hysteresis due to cyclic actuation.

Results and Discussion

While the ability of an elastomer to show evidence of actuation depends on the dielectric constant of the elastomer and the magnitude of the external electric field by eq 6, the extent to which the elastomer is able to respond to electrical stimulation is sensitive to the inherent mechanical properties of the elastomer. Previous studies[14−21] of triblock copolymer organogels containing MO, squalene, or another low-viscosity aliphatic additive have relied for the most part on dynamic rheology conducted in the linear viscoelastic limit (at low strain amplitudes) to extract dynamic shear moduli as functions of chemistry, copolymer concentration, and molecular weight for comparative purposes. Limited extensional rheometry has also been reported[22,39,41] for some selectively swollen copolymer networks. In this work, high deformation levels resulting from electrical actuation are anticipated, in which case we first turn our attention to tension and compression analyses of ENPs varying in copolymer concentration and molecular weight.

Nonlinear Mechanical Behavior. Representative stress−strain curves measured for triblock copolymer organogels varying in molecular weight and concentration, as well as the acrylic elastomer, under uniaxial tension are presented in Figure 2a. At the highest copolymer concentration displayed (30 wt % SEBS in MO), the organogels and acrylic elastomer exhibit qualitatively similar characteristics: a rapid initial rise that is gradually followed by a less pronounced monotonic increase in stress with increasing strain. The extensional behavior of the acrylic elastomer shows evidence of a second change in slope in the vicinity of 350% strain but is certainly comparable in magnitude to the ENP75 and ENP161 systems containing 30 wt % copolymer. At this concentration, which is common to all three copolymers, the mechanical behavior of the ENP75, ENP161, and ENP217 systems can be examined more closely to discern the molecular weight dependence. Since classic rubberlike (neo-Hookean) elasticity[42] fails to capture the stress−strain signatures evident in Figure 2a, we elect to analyze the data in terms of the slip-tube network (STN) model proposed by Rubinstein and Panyukov,[43] although we recognize that the semiempirical Mooney−Rivlin model[44] could also be used for this purpose. Within the context of the STN model,

$$\sigma = \left(G_c + \frac{G_e}{g(\lambda)}\right)\left(\lambda - \frac{1}{\lambda^2}\right) f(\phi, \Phi) \tag{10}$$

where σ is the nominal stress, and G_c and G_e represent contributions to G due to the existence of permanent cross-links and transient entanglements, respectively. The function $g(\lambda)$ is given by $0.74\lambda + 0.61\lambda^{-1/2} - 0.35$, where λ is the extension ratio, defined as L/L_0 (L_0 and L denote the specimen length before and after uniaxial extension, respectively) and related to strain by $\lambda - 1$.

For a solvent-swollen thermoplastic elastomer containing a dispersed solid filler, $f(\phi,\Phi)$ is a function of both filler concentration (ϕ) and copolymer volume fraction ($\Phi \approx w_{BC}$).[45,46] In the present case, however, ϕ is fixed by the copolymer composition (S content), which is nearly constant

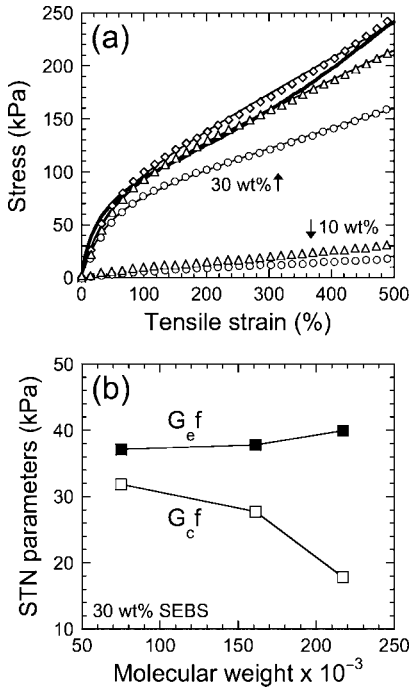

Figure 2. In (a), nominal (engineering) tensile stress−strain curves of three ENP systems—ENP75 (◇), ENP161 (△), and ENP217 (○)—evaluated at two copolymer concentrations: 10 and 30 wt % (labeled). In all cases, the extension rate was constant at 127 mm/min. The light solid lines correspond to regressed fits of the slip-tube network (STN) model[43] (eq 10) to the data, whereas the heavy solid line denotes the stress−strain response of the acrylic dielectric elastomer. In (b), parameters extracted from the STN model (labeled) are presented as functions of copolymer molecular weight at a constant copolymer concentration of 30 wt %. The solid lines serve to connect the data.

for the three copolymers in the SEBS series employed (30−33 wt % S), and Φ is necessarily constant since w_{BC} in the ENP series under investigation is set (at 30 wt % SEBS). Thus, $f(\phi,\Phi)$ is effectively a constant denoted here by f. Fitting eq 10 to the stress−strain data shown in Figure 2a yields excellent agreement, and regressed values of $G_c f$ and $G_e f$ are provided in Figure 2b, which reveals that G_c decreases, whereas G_e increases slightly, with increasing copolymer molecular weight at constant f. More importantly, however, the relative magnitudes of G_c and G_e indicate that entanglements, not cross-links, dominate G at 30 wt % copolymer. At lower w_{BC}, cross-links dominate and $G_c > G_e$. These results obtained from the nonlinear STN model establish that the ENPs under investigation in this study become increasingly stiffer due to their physically cross-linked networks as the copolymer molecular weight decreases at constant copolymer composition and gel concentration. Under these conditions, the copolymer molecular weight relates directly to the chain length between cross-links (micelles).

This trend is likewise apparent in Figure 3, which displays the dependence of the Young's tensile modulus (Y_T) on both copolymer concentration and molecular weight at ambient temperature. Conversely, as copolymer concentration is reduced in any of the three ENP series, Y_T decreases accordingly. Note that the ENP75 series does not form stable molecular networks at w_{BC} below ∼20 wt % copolymer. In all cases, however, it is important to recognize that the moduli values measured for the ENPs are consistently lower than that of the acrylic elastomer. Another important aspect of dielectric elastomers that can be gleaned from uniaxial tension testing is the mechanical hysteresis induced by cyclic deformation. Results acquired by subjecting the ENP161 and ENP217 systems with 10 and 30 wt % copolymer to 400% strain for 100 cycles are presented for illustrative purposes in Figure 5 to demonstrate that the present

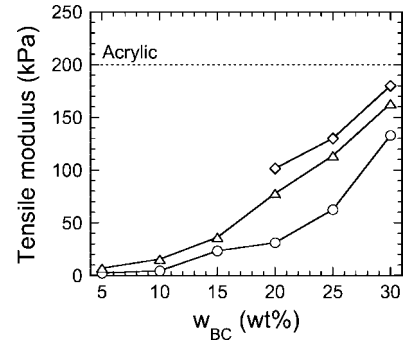

Figure 3. Dependence of the tensile modulus (Y_T) on copolymer concentration in the ENP75 (◇), ENP161 (△), and ENP217 (○) systems at ambient temperature. The solid lines connect the data, whereas the dashed line identifies the modulus for the acrylic elastomer.

ENPs do not generally exhibit pronounced hysteresis (<18% nonrecoverable strain) upon mechanical cycling at ambient temperature.[47] The ENP161 system with 5 wt % copolymer, which is close to the critical gel concentration required for network formation, fails prematurely (after 65 cycles), whereas the comparable ENP217 system remains intact with ∼1% nonrecoverable strain. Although the value of Y_T changes slightly with extension rate (from 100 to 500 mm/min), the corresponding degrees of hysteresis do not. In marked contrast, the permanent strain induced in the acrylic elastomer under identical cyclical conditions is ∼38%.

While the results from uniaxial tension testing provide insight into the molecular networks generated by triblock copolymer organogels under nonlinear elastic deformation conditions, compression testing is more closely related to the electromechanical deformation experienced by dielectric elastomers upon electrical actuation. Values of the compressive modulus (Y_C), discerned from the first linear region of the stress−strain curve after the initial transient arising from nonuniform contact between the platen and specimen surface, are presented as a function of copolymer concentration and molecular weight in Figure 5a and closely resemble the trends exhibited by Y_T in Figure 3. A direct comparison between Y_C and Y_T is included in Figure 5b and reveals that Y_C is consistently larger than Y_T by ∼75% on average. This deviation is attributed to the use of engineering stress in the calculation of Y_T in Figure 3. If, however, Y_T is determined from the true stress, which accounts for deformation-induced variation in cross-sectional area, the values of Y_C and Y_T are in substantially closer agreement, which is intuitively reasonable since values of Y_C are computed under the condition of constant specimen area (dictated by the probe size). The curves included in Figure 5a signify power-law fits of the form $Y_C = Y_C^0(w_{BC}/100)^n$, where Y_C^0 is the compressive modulus of the neat copolymer in the melt and n is a scaling exponent. The overall best-fit value for n is 2.0 (shown in Figure 5a), but regressed values range slightly from 1.9 to 2.3. For semidilute polymer solutions in the presence of a Θ or good solvent, n is theoretically expected to range from 2.25 to 2.33 but has been experimentally measured from 2.0 to 2.5,[20,22,45] which is consistent with the data reported here. Corresponding values of Y_C^0 range from 2.02 to 3.77 MPa. Under the condition that Poisson's ratio is 1/2, $Y_C \approx 3G$, which implies that the plateau shear modulus (G_N^0) of poly(ethylene-*co*-butylene), neglecting contributions from the S microdomains in the copolymer matrix, should be in the vicinity of 0.67−1.26 MPa at ambient temperature. This range agrees reasonably well with the measurements of Fetters et al.,[48] who report that G_N^0 for poly(ethylene-*alt*-butylene) is 0.58 MPa but increases to 0.69−1.12 MPa if the number of ethyl branches/100 carbon atoms along the backbone is less than 25, at 25 °C.

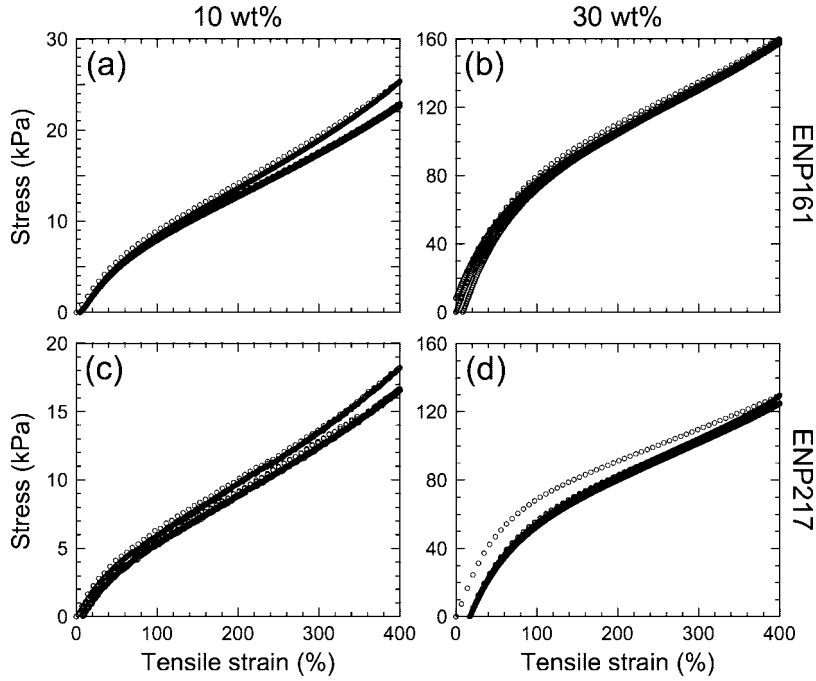

Figure 4. Nominal (engineering) tensile stress−strain curves measured from the ENP161 and ENP217 systems at 10 and 30 wt % copolymer concentrations (labeled) upon cycling 100 times to 400% strain. The degree of hysteresis is given by the nonrecoverable strain, the permanent deformation (shown as a shift in the data along the abscissa) introduced upon repeated extension.

The data presented in Figures 3−5 clearly indicate that the mechanical properties of ENPs can be readily tailored over a relatively broad range by judicious choice of copolymer molecular weight and concentration. This inherent versatility is in marked contrast to conventional dielectric elastomers derived from homopolymers, although we recognize that systematic changes in cross-link density in silicone elastomers, for instance, can likewise provide limited tunability (usually at the cost of detrimentally affecting electroresponsive behavior or stability). In addition, the very high tensile strains (>2000%) and strain energies achieved at failure for some of the ENPs further attest to the superior potential of triblock copolymer organogels as actuator materials. Since the Maxwell stress is compressive in nature, the electromechanical property evaluations reported in the next section will utilize the compressive modulus as required.

Electromechanical Behavior. As previously mentioned, the commercial acrylic adhesive presently constitutes the benchmark dielectric elastomer,[26] in which case direct comparisons between the ENPs and the acrylic elastomer will be provided throughout this section. Because of their lower rigidity, only the ENP161 and ENP217 systems will be considered further at this point. According to eq 6, electric-field-induced actuation depends on ϵ of the material as well as the applied electric field strength. Values of ϵ measured for the ENP161 and ENP217 series at ambient temperature are presented as a function of w_{BC} in Figure 6 and exhibit no discernible concentration dependence. These values are lower than those measured here for the acrylic elastomer and provided elsewhere[26] for both acrylic and silicone dielectric elastomers but are comparable in magnitude to those reported by Butkewitsch and Scheinbeim.[49] Unlike the acrylic elastomer, however, ϵ determined for the ENPs is virtually independent of frequency.[24] On the basis of the comparison provided in Figure 6 and the parameters required to generate a Maxwell stress (eq 6), the electromechanical response of the ENPs is naively anticipated to be lower than that of the acrylic and silicone elastomers. An important concept to recall before assessing actuation efficacy is that all dielectric elastomers are mechanically prestrained prior to electrical actuation to

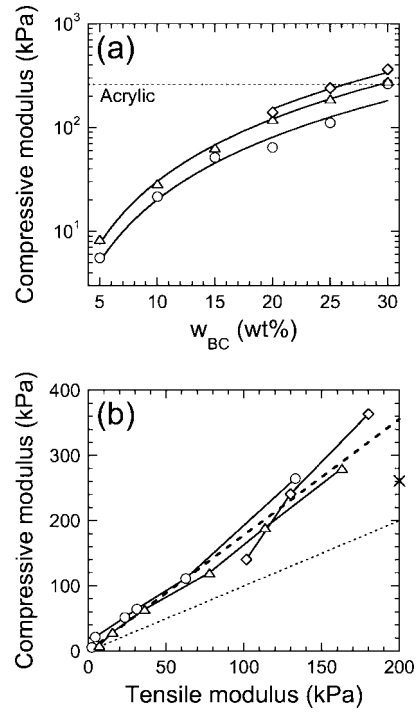

Figure 5. In (a), the compressive modulus (Y_C) presented as a function of copolymer concentration for the ENP75 (◊), ENP161 (△), and ENP217 (○) series. The solid lines are power-law fits to the data (with a scaling exponent of 2.0). The dashed line corresponds to the modulus measured for the acrylic dielectric elastomer. In (b), the compressive modulus is displayed in terms of the nominal (engineering) tensile modulus for the same ENP series as in (a). The solid lines serve to connect the data, whereas the dashed and dotted lines identify the best linear fit of the data and the condition where $Y_C = Y_T$, respectively. Included for comparison is a single datum point measured for the acrylic elastomer (×). Values of Y_C for the ENP75 systems are smaller in magnitude than those reported[24] earlier due to differences in test procedure (free compression here vs contact compression discussed in ref 40).

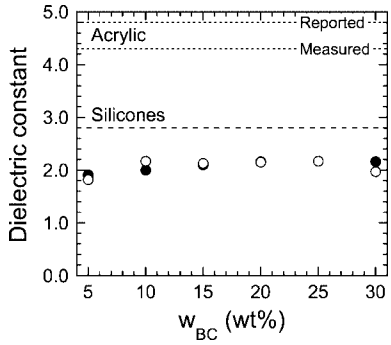

Figure 6. Dependence of the dielectric constant (ϵ) measured for the ENP161 (●) and ENP217 (○) series as a function of copolymer concentration. Included are data previously reported[26] and measured here for the acrylic dielectric elastomer, as well as data provided for silicone elastomers.

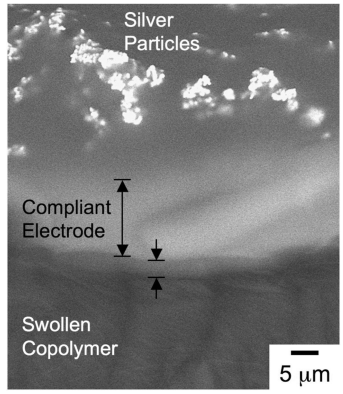

Figure 7. Cross-sectional BSE image of the ENP75 system with 35 wt % copolymer coated with a compliant electrode (Ag particles embedded in silicone). The MO-swollen copolymer is completely carbonaceous (dark), whereas the more electron-dense compliant electrode (arrow) appears light and the Ag particles within the electrode are bright. During fracture under liquid nitrogen, the pliable silicone layer forms protrusions, an example of which is seen in this image (arrowheads).

reduce specimen thickness and thus increase the magnitude of the electric field at constant voltage. (Prior studies[50] further indicate that ϵ can likewise be decreased through the use of mechanical prestrain, but this result remains open to general confirmation.) In keeping with this practice, the data reported below have been acquired from ENPs and the acrylic elastomer upon 300% biaxial prestrain using a home-built straining stage.[40]

After prestraining, compliant electrodes are applied to both sides of the film. A cross-sectional BSE image of the top portion of this layered construct is provided in Figure 7 and reveals that the electrode, which consists mainly of aggregated Ag particles (each measuring ~0.3 μm in diameter), is about 15−20 μm thick. The sharp delineation between the silicone-based electrode and the swollen copolymer film verifies that the electrode does not diffuse to any discernible extent into the copolymer film. Recall that s_{act} is measured directly from real-time images, such as the ones displayed for the ENP217 system with 5 wt % copolymer collected at initial and near dielectric breakdown (where the specimen fails) conditions in Figure 8. In this figure, s_{act} is also presented as a function of applied electric field for ENP217 systems differing in copolymer concentration. Several features of these data are particularly noteworthy. The first is that copolymer concentration has a systematic effect on the electromechanical response of the ENPs. At low w_{BC} (and correspondingly low modulus values), ultrahigh actuation strains (>200 area %) are achieved at relatively low

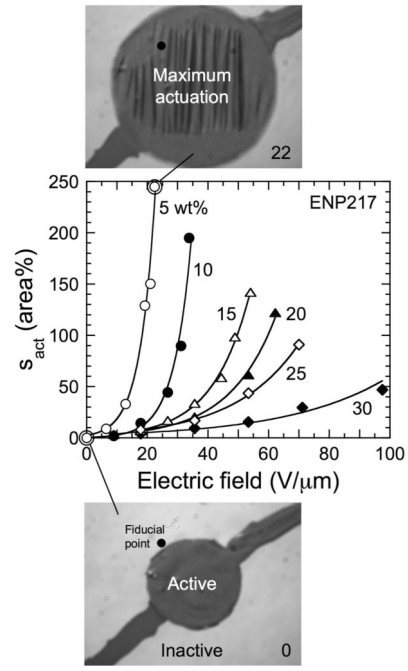

Figure 8. Actuation strain (s_{act}) measured for the ENP217 series (300% biaxial prestrain) as functions of applied electric field and copolymer concentration (labeled). The solid lines serve as guides for the eye. Images of the ENP217 systems containing 5 wt % copolymer correspond to pre-actuation (0 V/μm, bottom) and maximum actuation (22 V/μm, top). The active and inactive actuation areas, as well as a reference feature to facilitate comparison between the two images, are annotated in the bottom image.

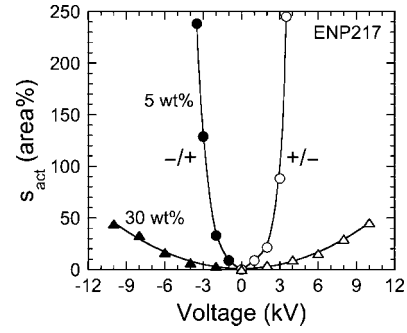

Figure 9. Dependence of the actuation strain (s_{act}) measured for the ENP217 series (300% biaxial prestrain) with 5 and 30 wt % copolymer (circles and triangles, respectively) at opposite electric polarities (labeled). The solid lines serve as guides for the eye.

electric field strengths (<40 V/μm). As w_{BC} is increased, however, the maximum s_{act} attained decreases, but the dielectric breakdown strength improves markedly. Complementary results provided in Figure 9 confirm that (i) the polarity of the applied electric potential has no effect on the magnitude of the ENP actuation response and, coupled with images such as those shown in Figure 8, (ii) electrical actuation of these ENPs occurs isotropically.

The images portrayed in Figure 8 illustrate that the active region of the ENP enlarges because the film thickness decreases due to the electric-field-induced development of a Maxwell stress. Maximum σ_M values, evaluated at the dielectric breakdown strengths measured from real-time video sequences in conjunction with eq 6, are displayed as a function of w_{BC} for the ENP161 and ENP217 series in Figure 10 and typically measure on the same order as the Y_C values in Figure 5. Included in this figure is the maximum σ_M value discerned for the acrylic

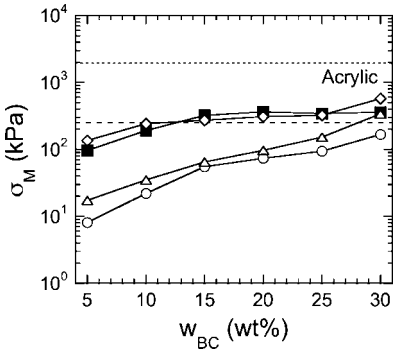

Figure 10. Maxwell stress (σ_M) as a function of copolymer concentration for the ENP161 (△, ◇) and ENP217 (○, ■) series (300% biaxial prestrain) evaluated at the dielectric breakdown field computed in terms of the initial specimen thickness (△, ○) and the true specimen thickness (◇, ■). Corresponding values measured for the acrylic elastomer (300% biaxial prestrain) are displayed as dashed and dotted lines, respectively.

elastomer. The nominal electric fields shown in Figure 8 and used to compute the σ_M values presented in Figure 10 are determined by dividing the applied voltage by the initial film thickness prior to actuation (t_0 in Figure 1a). While this is a standard convention, several efforts[26,33] have previously documented dielectric breakdown strengths on the basis of the true film thickness (t in Figure 1a). Corresponding σ_M values computed in this fashion by eq 9 and the definition of s_z are also provided in Figure 10. Since the method by which the dielectric breakdown field is calculated can account for more than an order of magnitude difference in σ_M at large actuation strains (low w_{BC}), caution must be exercised in drawing quantitative comparisons among actuation data tabulated for dielectric elastomers in the literature. Throughout the remainder of this study, all reported electric fields are nominal (i.e., computed relative to t_0). Another consideration that must be recognized is that the initial specimen thickness itself may likewise affect the measured actuation strain and breakdown field. We shall address this issue in a future report.

The dependence of the maximum actuation and transverse strains on w_{BC} for the ENP161 and ENP217 series containing MO is shown in Figure 11, parts a (s_{act}) and b ($|s_z|$). In both cases, the electric-field-induced displacements decrease monotonically with increasing w_{BC} and, at the lowest w_{BC} examined here, exceed the actuation performance of both the acrylic and silicone dielectric elastomers. The MO employed in all the organogels discussed thus far contains a non-negligible naphthenic fraction (~30%) that may exhibit limited compatibility with the S end blocks of the copolymers and consequently locate within (and plasticize) the glassy micelles at ambient temperature.[15] The extent of micelle deformation during prestrain and actuation in ENPs is an important consideration currently under investigation. The results presented in Figure 11 indicate that the ENP217/MO series consistently attains greater electric-field-induced displacement than the ENP161/MO series, thereby establishing that the ENP series with the lower modulus exhibits the larger electromechanical response. Conversely, the series achieving larger actuation displacement displays the lower dielectric breakdown field, as evidenced in Figure 12a. At high w_{BC}, the breakdown fields measured for both ENP series are comparable to those reported[26] for silicone and acrylic dielectric elastomers. At low w_{BC}, however, the glassy micelles are separated by greater distance due to a higher degree of swelling, and the breakdown fields of both ENP series are considerably lower, suggesting that the MO limits dielectric breakdown. For completeness, the maximum s_{act} is provided as a function of breakdown field for the ENP161/MO and ENP217/MO series, the acrylic elastomer, and two different silicone elastomers in

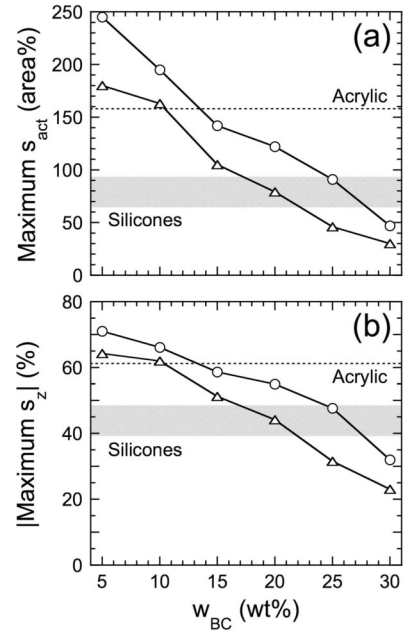

Figure 11. Maximum actuation and transverse strains (s_{act} and $|s_z|$, respectively) presented as functions of copolymer concentration for the ENP161/MO (△) and ENP217/MO (○) series (300% biaxial prestrain) in (a) and (b), respectively. The solid and dashed lines serve to connect the data, whereas the dotted line and shaded region correspond to acrylic (300% biaxial prestrain) and silicone dielectric elastomers,[26] respectively.

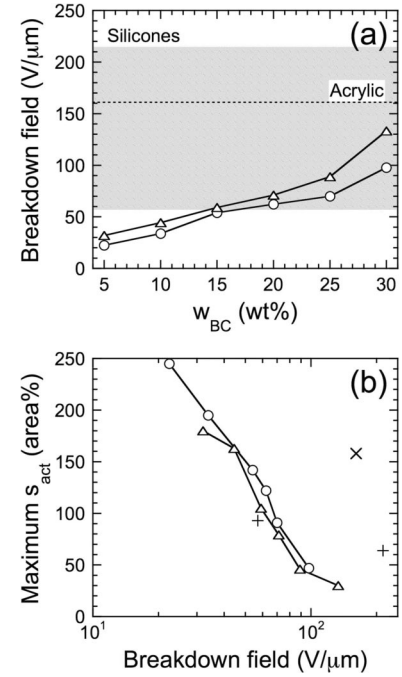

Figure 12. In (a), the dielectric breakdown field (relative to the initial specimen thickness) displayed as a function of copolymer concentration for the ENP161/MO (△) and ENP217/MO (○) series (300% biaxial prestrain). The solid and dashed lines serve to connect the data, whereas the dotted line and shaded region correspond to acrylic (300% biaxial prestrain) and silicone dielectric elastomers,[26] respectively. In (b), the maximum actuation strain shown in terms of the dielectric breakdown field for the same series as in (a). The acrylic (×) and silicone (+) elastomers are included for comparison.

Figure 12b. It is interesting to note that results from the ENP series containing MO overlap. Included in Figure 12b are data reported[26] for the acrylic elastomer (at high displacement, 158

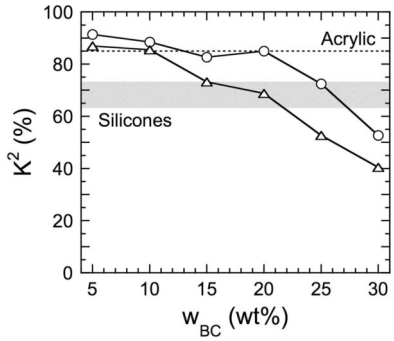

Figure 13. Dependence of the electromechanical coupling efficiency (K^2) on copolymer concentration for the ENP161/MO (△) and ENP217/MO (○) series (300% biaxial prestrain). The solid and dashed lines serve to connect the data, whereas the dotted line and shaded region correspond to acrylic (300% biaxial prestrain) and silicone dielectric elastomers,[26] respectively.

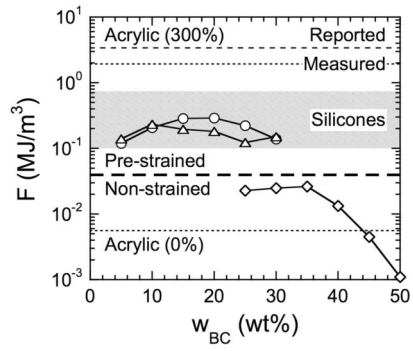

Figure 14. Energy density (F) values displayed as a function of copolymer concentration for the ENP161/MO (△) and ENP217/MO (○) series. The light dashed and dotted lines (labeled) and the shaded region correspond to acrylic and silicone dielectric elastomers,[26] respectively. Dielectric elastomers shown above the heavy dashed line have been subjected to mechanical prestrain (300% biaxial for both the ENP and acrylic elastomers) prior to actuation. At conditions included below the heavy dashed line, the ENP75 (◊) and acrylic elastomers are relaxed (0% prestrain) prior to actuation. The solid lines serve to connect the data.

area %, and high field, 161 V/μm) and a silicone elastomer (at low displacement and high field).

Another metric of dielectric elastomer actuation performance is the electromechanical coupling efficiency (K^2), defined[25,26] as the ratio of stored mechanical energy to input electrical energy. This parameter provides a measure of energy conversion efficiency and is related to s_z by

$$K^2 = -2s_z - {s_z}^2 \tag{11}$$

The dependence of K^2 on w_{BC} for the ENP161/MO and ENP217/MO series, along with both acrylic and silicone elastomers, is displayed in Figure 13 and reveals that K^2 generally decreases with increasing w_{BC}. The results shown in this figure confirm that the ENPs introduced here attain efficiencies that are comparable, if not superior, to existing dielectric elastomers. The low-modulus ENPs with the largest s_{act} achieved possess the highest K^2 values reported to date (for the ENP217 system containing 5 wt % copolymer, $K^2 \approx 92\%$). Moreover, K^2 is found to decrease with decreasing copolymer molecular weight over the entire concentration range examined. The energy density (F) complements K^2 by providing a measure of the work generated per actuation cycle per unit volume of actuator (exclusive of overhead peripherals).[51] At large actuation strains such as those observed with the ENPs, as well as acrylic and silicone elastomers, F is given by

$$F = -\sigma_M \ln(1 + s_z) \tag{12}$$

Values of F determined for both ENP/MO series are provided as a function of w_{BC} in Figure 14 and compare favorably with those determined for silicone elastomers. These values are, however, lower than those of the acrylic elastomer: reported[26] as 3.4 MJ/m^3 and measured as 1.9 MJ/m^3.

All the ENPs discussed thus far require a large mechanical prestrain (uniaxial or biaxial) to realize their superior actuation performance. As discussed elsewhere,[24] prestraining an elastomer film can promote net reductions in the quality of actuation performance (due to stress relaxation of the elastomer over time) and the life of the elastomer (due to prolonged stress concentration along the elastomer/frame interface). We have recently reported that, due to its intrinsic rigidity (cf. Figures 3 and 5), the ENP75/MO series undergoes only moderate actuation ($s_{act} < 20$ area % and $K^2 < 30\%$) without mechanical prestrain prior to actuation. At small actuation strain levels, F can be assessed directly from Hooke's law,[24,25] in which case $F = Y_C {s_z}^2/2$. Included in Figure 14 to illustrate the importance of mechanical prestrain in the actuation efficacy of dielectric elastomers are values of F measured for the ENP75/MO series and the acrylic elastomer without mechanical prestrain prior to actuation. While a considerable reduction in F is evident in the absence of mechanical prestrain, the ENP75 series nonetheless outperforms the acrylic elastomer over most of the copolymer concentration range explored. The abrupt decrease in F in the ENP75 series with increasing w_{BC} may reflect an increase in the extent of entangled loops along the coronas of the glassy micelles or the onset of microphase ordering, both of which could inhibit deformation of the copolymer network upon actuation. While this feature remains under investigation, the results displayed in Figure 14 nonetheless confirm that a tradeoff in ENP actuation performance exists: ultrahigh s_{act} and K^2 increase at the expense of F and vice versa.

Conclusions

Because of their exceptional adhesive, shape-memory, and vibration-dampening attributes, triblock copolymer organogels have found tremendous use in a wide range of present-day technologies. In this work, we demonstrate that they are likewise stimulus-responsive materials that can be used as dielectric elastomers in the lightweight, flexible, and efficient actuators required in the ongoing development of microrobotic systems (e.g., micro-air vehicles), microfluidic/haptic/biomedical devices (e.g., active Braille and steerable catheters), and smart prosthetics. The electromechanical data reported here confirm the robust mechanical properties (low hysteresis, high strain cycling, and very high failure strains) and broadly tunable actuation performance of ENPs. Unlike conventional dielectric elastomers derived from chemically cross-linked homopolymers, the present ENPs rely on the microphase-separated network morphology afforded by selectively swollen triblock copolymers, the electromechanical properties of which can be systematically altered through variation in copolymer parameters (i.e., molecular composition, organogel concentration, and molecular weight) and/or solvent quality. In this regard, further studies are clearly warranted to elucidate the underlying nanostructure−property relationships governing actuation performance. The relatively nonpolar ENP systems investigated in this work exhibit high actuation strains and coupling efficiencies at relatively low electric fields, which makes them particularly suited for energy-efficient applications requiring substantial displacement with little pushing or pulling. Equally important, these

materials compare favorably relative to the benchmark acrylic dielectric elastomer, as well as to various silicone elastomers, and even show evidence of modest actuation in the absence of mechanical prestrain. A major shortcoming of current dielectric elastomers is their inability to produce significant force to accompany large actuation strains, which is why much recent attention has been paid to the development of high-modulus electrostrictive polymers.[29,30] By tailoring the molecular and bulk properties of the copolymer and midblock-selective solvent independently, however, the ENP design strategy described herein provides an attractive and viable route to high-performance dielectric materials with physically tunable electromechanical properties.

Acknowledgment. This work was supported by the U.S. Department of Commerce through the National Textiles Center.

References and Notes

(1) Hamley, I. W. *The Physics of Block Copolymers*; Oxford University Press: New York, 1998. Bates, F. S.; Fredrickson, G. H. *Phys. Today* **1999**, *52*, 32. Abetz, V. In *Encyclopedia of Polymer Science and Technology*, 3rd ed.; Kroschwitz, J. I., Ed.; Wiley: Hoboken, NJ, 2003; Vol. *1*, pp 482−523.

(2) Holden, G., Kricheldorf, H. R., Quirk, R. P., Eds.; *Thermoplastic Elastomers*, 3rd ed.; Hanser: Munich, 2004.

(3) Mayes, A. M.; Olvera de la Cruz, M. *J. Chem. Phys.* **1989**, *91*, 7228. Dobrynin, A. V.; Erukhimovich, I. Ya. *Macromolecules* **1993**, *26*, 276. Matsen, M. W.; Thompson, R. B. *J. Chem. Phys.* **1999**, *111*, 7139.

(4) Laurer, J. H.; Hajduk, D. A.; Fung, J. C.; Sedat, J. W.; Smith, S. D.; Gruner, S. M.; Agard, D. A.; Spontak, R. J. *Macromolecules* **1997**, *30*, 3938.

(5) Falus, P.; Xiang, H.; Borthwick, M. A.; Russell, T. P.; Mochrie, S. G. J. *Phys. Rev. Lett.* **2004**, *93*, 145701.

(6) Park, C.; Yoon, J.; Thomas, E. L. *Polymer* **2003**, *44*, 6725. Hamley, I. W. *Angew. Chem., Int. Ed.* **2003**, *42*, 1692.

(7) Lazzari, M., Liu, G., Lecommandoux, S., Eds.; *Block Copolymers in Nanoscience*; Wiley-VCH: Weinheim, 2006.

(8) Templin, M.; Franck, A.; DuChesne, A.; Leist, H.; Zhang, Y. M.; Ulrich, R.; Schadler, V.; Wiesner, U. *Science* **1997**, *278*, 1795. Zhao, D. Y.; Feng, J. L.; Huo, Q. S.; Melosh, N.; Fredrickson, G. H.; Chmelka, B. F.; Stucky, G. D. *Science* **1998**, *279*, 548. Hedrick, J. L.; Miller, R. D.; Hawker, C. J.; Carter, K. R.; Volksen, W.; Yoon, D. Y.; Trollsås, M. *Adv. Mater.* **1998**, *10*, 1049.

(9) Arnold, M. E.; Nagai, K.; Spontak, R. J.; Freeman, B. D.; Leroux, D.; Betts, D. E.; DeSimone, J. M.; DiGiano, F. A.; Stebbins, C. K.; Linton, R. W. *Macromolecules* **2002**, *35*, 3697. Patel, N. P.; Spontak, R. J. *Macromolecules* **2004**, *37*, 2829. Spontak, R. J.; Shankar, R.; Bowman, M. K.; Krishnan, A. S.; Hamersky, M. W.; Samseth, J.; Bockstaller, M. R.; Rasmussen, K. Ø. *Nano Lett.* **2006**, *6*, 2115.

(10) Pai, R. A.; Raashina, H.; Schulberg, M. T.; Sengupta, A.; Sun, J.-N.; Watkins, J. J. *Science* **2004**, *303*, 5. Yokoyama, H.; Li, L.; Nemoto, T.; Sugiyama, K. *Adv. Mater.* **2004**, *16*, 1542. Hillmyer, M. A. *Adv. Polym. Sci.* **2005**, *190*, 137.

(11) Tsuruta, T. *Adv. Polym. Sci.* **1996**, *126*, 1. Duncan, R. *Nat. Rev. Drug Discovery* **2003**, *2*, 347. Alarcon, C. D. H.; Pennadam, S.; Alexander, C. *Chem. Soc. Rev.* **2005**, *34*, 276.

(12) Spontak, R. J.; Patel, N. P. *Curr. Opin. Colloid Interface Sci.* **2000**, *5*, 334. Holden, G. *Understanding Thermoplastic Elastomers*; Hanser: Munich, 2000.

(13) Lodge, T. P.; Hamersky, M. W.; Hanley, K. J.; Huang, C.-I. *Macromolecules* **1997**, *30*, 6139. Hanley, K. J.; Lodge, T. P.; Huang, C.-I. *Macromolecules* **2000**, *33*, 5918. Lodge, T. P.; Pudil, B.; Hanley, K. J. *Macromolecules* **2002**, *35*, 4707. Lodge, T. P.; Hanley, K. J.; Pudil, B.; Alahapperuma, V. *Macromolecules* **2003**, *36*, 816.

(14) Laurer, J. H.; Khan, S. A.; Spontak, R. J.; Satkowski, M. M.; Grothaus, J. T.; Smith, S. D.; Lin, J. S. *Langmuir* **1999**, *15*, 7947.

(15) Laurer, J. H.; Bukovnik, R.; Spontak, R. J. *Macromolecules* **1996**, *29*, 5760. Laurer, J. H.; Mulling, J. F.; Khan, S. A.; Spontak, R. J.; Lin, J. S.; Bukovnik, R. *J. Polym. Sci., Part B: Polym. Phys.* **1998**, *36*, 2513. Laurer, J. H.; Mulling, J. F.; Khan, S. A.; Spontak, R. J.; Bukovnik, R. *J. Polym. Sci., Part B: Polym. Phys.* **1998**, *36*, 2379.

(16) Jackson, N. R.; Wilder, E. A.; White, S. A.; Bukovnik, R.; Spontak, R. J. *J. Polym. Sci., Part B: Polym. Phys.* **1999**, *37*, 1863. Spontak, R. J.; Wilder, E. A.; Smith, S. D. *Langmuir* **2001**, *17*, 2294. Wilder, E. A.; White, S. A.; Smith, S. D.; Spontak, R. J. *ACS Symp. Ser.* **2002**, *833*, 248. van Maanen, G. J.; Seeley, S. L.; Capracotta, M. D.; White, S. A.; Bukovnik, R. R.; Hartmann, J.; Martin, J. D.; Spontak, R. J. *Langmuir* **2005**, *21*, 3106.

(17) Soenen, H.; Berghmans, H.; Winter, H. H.; Overbergh, N. *Polymer* **1997**, *38*, 5653. Soenen, H.; Liskova, A.; Reynders, K.; Berghmans, H.; Winter, H. H.; Overbergh, N. *Polymer* **1997**, *38*, 5661.

(18) Mischenko, N.; Reynders, K.; Mortensen, K.; Scherrenberg, R.; Fontaine, F.; Graulus, R.; Reynaers, H. *Macromolecules* **1994**, *27*, 2345. Reynders, K.; Mischenko, N.; Mortensen, K.; Overbergh, N.; Reynaers, H. *Macromolecules* **1995**, *28*, 8699. Mischenko, N.; Reynders, K.; Koch, M. H. J.; Mortensen, K.; Pedersen, J. S.; Fontaine, F.; Graulus, R.; Reynaers, H. *Macromolecules* **1995**, *28*, 2054. Mortensen, K.; Theunissen, E.; Kleppinger, R.; Almdal, K.; Reynaers, H. *Macromolecules* **2002**, *35*, 7773. Mortensen, K. *J. Polym. Sci., Part B: Polym. Phys.* **2004**, *42*, 3095.

(19) Quintana, J. R.; Diaz, E.; Katime, I. *Macromolecules* **1997**, *30*, 3507; *Polymer* **1998**, *39*, 3029. Quintana, J. R.; Janez, M. D.; Hernaez, E.; Garcia, A.; Katime, I. *Macromolecules* **1998**, *31*, 6865. Quintana, J. R.; Hernaez, E.; Katime, I. *Polymer* **2002**, *43*, 3217.

(20) Vega, D. A.; Sebastian, J. M.; Loo, Y. L.; Register, R. A. *J. Polym. Sci., Part B: Polym. Phys.* **2001**, *39*, 2183.

(21) Watanabe, H. *Macromolecules* **1995**, *28*, 5006. Karatasos, K.; Anastasiadis, S. H.; Pakula, T.; Watanabe, H. *Macromolecules* **2000**, *33*, 523. Watanabe, H.; Tan, H. *Macromolecules* **2004**, *37*, 5118.

(22) Roos, A.; Creton, C. *Macromolecules* **2005**, *38*, 7807.

(23) Shankar, R.; Ghosh, T. K.; Spontak, R. J. *Adv. Mater.* **2007**, *19*, 2218.

(24) Shankar, R.; Ghosh, T. K.; Spontak, R. J. *Macromol. Rapid Commun.* **2007**, *28*, 1142.

(25) Shankar, R.; Ghosh, T. K.; Spontak, R. J. *Soft Matter* **2007**, *3*, 1116.

(26) Pelrine, R.; Kornbluh, R.; Pei, Q.; Joseph, J. *Science* **2000**, *287*, 836.

(27) Bar-Cohen, Y., Ed. *Electroactive Polymer (EAP) Actuators as Artificial Muscles: Reality, Potential, and Challenges*; SPIE Press: Bellingham, WA, 2004. Bar-Cohen, Y. In *Biomimetics: Biologically Inspired Technologies*; Bar-Cohen, Y., Ed.; CRC Press/Taylor & Francis: Boca Raton, FL, 2005. Mirfakhrai, T.; Madden, J. D. W.; Baughman, R. H. *Mater. Today* **2007**, *10*, 30.

(28) Pons, J. L. *Emerging Actuator Technologies: A Micromechatronic Approach*; Wiley: Hoboken, NJ, 2005.

(29) Zhang, Q. M.; Bharti, V.; Zhao, X. *Science* **1998**, *280*, 2101. Zhang, Q. M.; Li, H.; Poh, M.; Xia, F.; Cheng, Z.-Y.; Xu, H.; Huang, C. *Nature (London)* **2002**, *419*, 284. Xia, F.; Cheng, Z. Y.; Xu, H. S.; Li, H. F.; Zhang, Q. M.; Kavarnos, G. J.; Ting, R. Y.; Abdul-Sedat, G.; Belfield, K. D. *Adv. Mater.* **2002**, *14*, 1574.

(30) Lehmann, W.; Skupin, H.; Tolksdorf, C.; Gebhard, E.; Zentel, R.; Kruger, P.; Losche, M.; Kremer, F. *Nature (London)* **2001**, *410*, 447. Casalini, R.; Roland, C. M. *Appl. Phys. Lett.* **2001**, *79*, 2627. Roland, C. M.; Garrett, J. T.; Casalini, R.; Roland, D. F.; Santangelo, P. G.; Qadri, S. B. *Chem. Mater.* **2004**, *16*, 857. Berdichevsky, Y.; Lo, Y. H. *Adv. Mater.* **2006**, *18*, 122.

(31) Baughman, R. H.; Cui, C.; Zakhidov, A. A.; Iqbal, Z.; Barisci, J. N.; Spinks, G. M.; Wallace, G. G.; Mazzoldi, A.; De Rossi, D.; Rinzler, A. G.; Jaschinski, O.; Roth, S.; Kertesz, M. *Science* **1999**, *284*, 1340. Madden, J. D. W.; Barisci, J. N.; Anquetil, P. A.; Spinks, G. M.; Wallace, G. G.; Baughman, R. H.; Hunter, I. W. *Adv. Mater.* **2006**, *18*, 870.

(32) Because of the circular geometry routinely employed in the actuation characterization of dielectric elastomers, displacements are normally reported on an area basis. For brevity, this basis will be expressed as area % in the present work.

(33) Pelrine, R.; Kornbluh, R.; Kofod, G. *Adv. Mater.* **2000**, *12*, 1223.

(34) Morkved, T. L.; Lu, M.; Urbas, A. M.; Ehrichs, E. E.; Jaeger, H. M.; Mansky, P.; Russell, T. P. *Science* **1996**, *273*, 931. Xu, T.; Zvelindovsky, A. V.; Sevink, G. J. A.; Lyakhova, K. S.; Jinnai, H.; Russell, T. P. *Macromolecules* **2005**, *38*, 10788.

(35) Böker, A.; Elbs, H.; Hänsel, H.; Knoll, A.; Ludwigs, S.; Zettl, H.; Urban, V.; Abetz, V.; Müller, A. H.; Krausch, G. *Phys. Rev. Lett.* **2002**, *89*, 135502. Böker, A.; Elbs, H.; Hansel, H.; Knoll, A.; Ludwigs, S.; Zettl, H.; Zvelindovsky, A. V.; Sevink, G. J. A.; Urban, V.; Abetz, V.; Muller, A. H. E.; Krausch, G. *Macromolecules* **2003**, *36*, 8078.

(36) Cheng, L.-T.; Tam, W.; Marder, S. R.; Stiegman, A. E.; Rikken, G.; Spangler, C. W. *J. Phys. Chem.* **1991**, *95*, 10643.

(37) Pelrine, R.; Kornbluh, R.; Joseph, J.; Heydt, R.; Pei, Q. B.; Chiba, S. *Mater. Sci. Eng., C* **2000**, *11*, 89. Wissler, M.; Mazza, E. *Sens. Actuators A* **2005**, *120*, 184. Palakodeti, R.; Kessler, M. R. *Mater. Lett.* **2006**, *60*, 3437.

(38) Yang, G.; Yao, G.; Ren, W.; Akhras, G.; Szabo, J. P.; Mukherjee, B. K. *Proc. SPIE* **2005**, *5759*, 134.

(39) Prasman, E.; Thomas, E. L. *J. Polym. Sci., Part B: Polym. Phys.* **1998**, *36*, 1625.

(40) Shankar, R.; Ghosh, T. K.; Spontak, R. J. *Sens. Actuators A*, in press.

(41) Kleppinger, R.; van Es, M.; Mischenko, N.; Koch, M. H. J.; Reynaers, H. *Macromolecules* **1998**, *31*, 5805.

(42) Gent, A. N. In *Engineering with Rubber*; Gent, A. N., Ed.; Hanser: Munich, 1992; pp 33−66.

(43) Rubinstein, M.; Panyukov, S. *Macromolecules* **2002**, *35*, 6670.

(44) Mooney, M. *J. Appl. Phys.* **1940**, *11*, 582. Rivlin, R. S. *Philos. Trans. R. Soc. London, Ser. A* **1948**, *241*, 379.
(45) Guth, E. *J. Appl. Phys.* **1945**, *16*, 20.
(46) de Gennes, P. G. *Scaling Concepts in Polymer Physics*; Cornell University Press: New York, 1979.
(47) Chen, Y. D. M.; Cohen, R. E. *J. Appl. Polym. Sci.* **1977**, *21*, 629.
(48) Fetters, L. J.; Lohse, D. J.; Richter, D.; Witten, T. A.; Zirkel, A. *Macromolecules* **1994**, *27*, 4639.
(49) Butkewitsch, S.; Scheinbeim, J. *Appl. Surf. Sci.* **2006**, *252*, 8277.
(50) Choi, H. R.; Jung, K.; Chuc, N. H.; Jung, M.; Koo, I.; Koo, J.; Lee, J.; Lee, J.; Nam, J.; Cho, M. *Proc. SPIE* **2005**, *5759*, 283.
(51) Madden, J. D. W.; Vandesteeg, N. A.; Anquetil, P. A.; Madden, P. G. A.; Takshi, A.; Pytel, R. Z.; Lafontaine, S. R.; Wieringa, P. A.; Hunter, I. W. *IEEE J. Oceanic Eng.* **2004**, *29*, 706.

MA071903G